Unsteady dynamics of wedge-induced oblique detonations under periodic inflows

Pengfei Yang (杨鹏飞) [1,2,3], Hoi Dick Ng [4] and Honghui Teng (滕宏辉) [2,a]

[1] School of Aerospace Engineering, Beijing Institute of Technology, Beijing 100081, China

[2] State Key Laboratory of High Temperature Gas Dynamics, Institute of Mechanics, Chinese Academy of Sciences, Beijing 100190, China

[3] School of Engineering Sciences, University of Chinese Academy of Sciences, Beijing 100049, China

[4] Department of Mechanical, Industrial and Aerospace Engineering, Concordia University, Montreal, Quebec, H3G 1M8, Canada

Abstract:

Two-dimensional, wedge-induced oblique detonation waves (ODWs) subject to periodic inflow are simulated using the reactive Euler equations with a two-step induction–reaction kinetic model. The focus of this work is how the periodic unsteadiness of a sinusoidal density disturbance with varying frequency and amplitude influences an initially established ODW structure. Three fundamental ODW structures with different transition types and inflow Mach numbers are disturbed, resulting in two types of triple-point formations: the main triple point (MTP) and the train of triple points (TTP). The TTP features multi-triple points arising almost simultaneously and travelling together, which has never been observed before. Parametric study and frequency analysis reveal that the MTP derives from forced destabilisation, while the TTP derives from the combined effect of surface instability and inflow disturbance. Furthermore, a new phenomenon of the MTP degeneration is observed for a proper inflow Mach number and disturbance amplitude. Finally, the oscillation amplitudes of unsteady ODWs are analysed with respect to Mach number and inflow disturbance, demonstrating the effects of transition type on the surface unsteadiness.

Key words: Oblique detonation, induction–reaction kinetics, initiation, triple points, unstable surface

---

[a] Author to whom correspondence should be addressed: hhteng@bit.edu.cn

1. Introduction

Detonation-based engines have attracted increasing attention in recent years[1]. Among these is the oblique detonation engine (ODE) with its potential for hypersonic propulsion. Achieving steady ODE operation requires fundamental knowledge of the initiation and stability of an oblique detonation wave (ODW). The ODW is a classical problem studied analytically since the 1960s (see this reference[2] and references therein). Subsequent numerical and experimental studies[3,4] have shown that an inert oblique shock wave (OSW) essentially exists upstream, inducing an OSW–ODW transition viewed as ODW initiation. The ODW research appears to focus on different aspects since then, involving the OSW–ODW transitions[5−8], the ODW surface instability[9−15] and the ODW interactions with complicated geometry[16−19]. However, most of these studies were performed assuming steady and uniform inflow conditions.

The uniform inflow assumption was first relaxed by modelling inflow inhomogeneity with different spatial equivalence ratio distributions, resulting in a distorted ODW reactive front[20,21]. The effects of unsteadiness were investigated by introducing a large discrete density disturbance in the flow or abruptly changing the wedge angle to elucidate complex ODW evolution and hysteresis as well as transitions between different steady structures[22,23]. ODW dynamics in continuous unsteady inflow was investigated recently[24] by imposing a sinusoidal inflow density disturbance with different frequencies. The triple points were generated by the inflow disturbance, and the ODW oscillated with the same inflow disturbance frequency, although the oscillation amplitude varied with position and disturbance frequency. Further analysis revealed a resonance-like ODW oscillation, illustrating the overshooting oscillation of the downstream surface for a modest disturbance frequency.

To gain further insights on ODW initiation and stability subject to unsteady inflow, this work studies how the periodic unsteadiness of a sinusoidal density disturbance influences an initially established ODW structure. The previous study[24] was based on fixed values of the inflow Mach number M_0 and disturbance amplitude A, with the disturbance frequency as the main bifurcation parameter. In the present study, both M_0 and A are variable besides the disturbance frequency. Thus, a richer and systematic description of the unsteady ODW dynamics can be obtained from numerous results, also revealing phenomena not observed before. Two mechanisms of triple-point formation are proposed from the flow dynamics, completing the understanding of surface unsteadiness. The oscillation amplitudes are analysed in detail, revealing the effects of transition type on surface unsteadiness.

2. Methodology

2.1 Numerical and mathematical models

Following the canonical ODW simulation setting[11–13,24,25], the reactive Euler equations are used coupled with a two-step model for chain-branching kinetics[26,27]:

$$\dot{\omega}_1 = H(1 - \xi)\rho k_I \exp\left[E_I\left(\frac{1}{T_S} - \frac{1}{T}\right)\right] \tag{1}$$

$$\dot{\omega}_2 = [1 - H(1 - \xi)]\rho(1 - \eta)k_R \exp\left[-\frac{E_R}{T}\right] \tag{2}$$

where $\dot{\omega}_1$ and $\dot{\omega}_2$ represent the reaction rate of the induction zone and heat release zone, respectively; ξ and η represent the progress variables for the induction and reaction steps; $H(1–\xi)$ is a Heaviside step function (1 when $\xi \leq 1$ or 0 if $\xi > 1$); e is the specific total energy given by $p/[\rho(\gamma-1)]$ + $(u^2 + v^2)/2 - \eta Q$; ρ, u, v, p, e, and Q are the density, velocities in the x- and y-directions, pressure, specific total energy, and specific heat release, respectively, all scaled with the uniform unburned state[8,24,27] as follows:

$$\rho = \frac{\tilde{\rho}}{\rho_0}, \quad p = \frac{\tilde{p}}{p_0}, \quad T = \frac{\tilde{T}}{T_0}, \quad u = \frac{\tilde{u}}{\sqrt{RT_0}}, \quad v = \frac{\tilde{v}}{\sqrt{RT_0}}, \quad Q = \frac{\tilde{Q}}{RT_0} \tag{3}$$

The main parameters are, $Q = 50$, $\gamma = 1.2$, $E_I = 5.0\ T_s$, and $E_R = 1.0\ T_s$, where T_s is the post-shock temperature of the one-dimensional Chapman–Jouguet (CJ) detonation, and the activation energies E_I and E_R have been scaled with RT_0. Two kinetic parameters, k_I and k_R, are necessary to complete the model: k_R is fixed to 1.0, while $k_I = -u_{vn}$, where u_{vn} is the particle velocity behind the shock front in the shock-fixed frame for the one-dimensional CJ detonation. Thus, the induction length of the one-dimensional CJ detonation is chosen as the reference length scale L_{ref} and is fixed to unity. The reference time scale is therefore defined as the ratio of the reference length scale divided by the initial sound speed of the reactant [27]. The heat release amount and specific heat ratio of the reactive mixture, i.e. $Q = 50$ and $\gamma = 1.2$, are employed widely in earlier studies based on the typical Arrhenius kinetic model[11,14,27]. The Mach number of CJ detonation is 6.22 for the mixture in the present study, which is a little larger than the stoichiometric hydrogen-oxygen mixture. The typical value of the induction activation energy usually ranges from $4T_s$ to $12T_s$ for hydrocarbon mixtures[27]. Nonetheless, these chemical parameters do not correspond readily to any detailed reactants. The chosen parameters can result in a weakly unstable normal detonation[27], which is further stabilized in the ODW setting due to the overdrive. The two-step model, consisting of a thermally neutral induction step followed by the main heat release reaction layer, is detailed enough to retain the features of real combustion governed by chain branching kinetics. More importantly, such a model involves two length scales, i.e. induction and reaction lengths, which can be varied independently to change the sensitivity and flow structure of the chemical reaction zone.

The governing equations are numerically solved using the dispersion-controlled dissipation (DCD) scheme[28] with a third-order Runge–Kutta algorithm. The DCD adjusts the dispersion around

a strong discontinuity, and thus around suppressed non-physical oscillations near the shock. It is one kind of total variation diminishing scheme which can achieve second-order accuracy in a smooth flow field. To solve the chemical reaction, we use a fractional step algorithm where the non-reacting flow is computed first for a time step, then the chemical reaction is integrated into the flow. To verify the grid resolution and convergence, the steady/unsteady ODWs are examined with different grid scales and the resulting flow fields are shown and discussed in Appendix A. Besides, the zoom-in density contours for the unsteady ODW with the progress variables η of the heat release reaction are also plotted to show the flow details around the triple points. Hence, the grid resolution, $dx = 0.10$, can be given in terms of the characteristic reaction length scales of detonation waves.

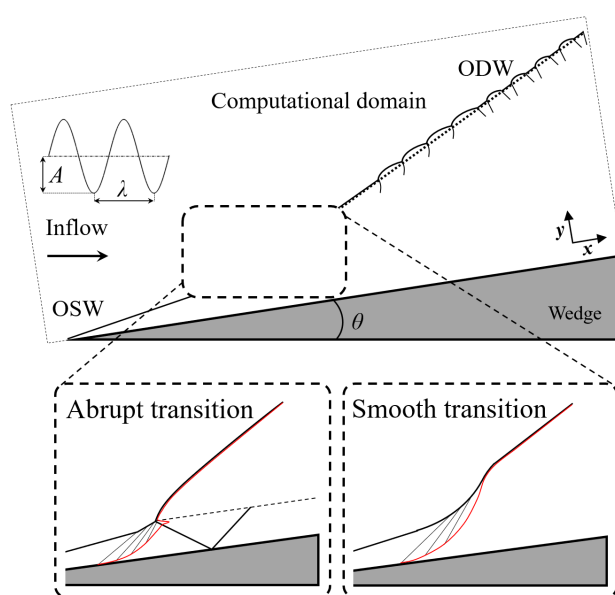## 2.2 Periodic inflows and disturbance frequency

FIG. 1. Schematic of ODW in periodic inflow

Figure 1 shows the computation settings with the Cartesian domain rotated and aligned with the wedge. Hence, the incoming flow velocity from the boundaries thus has components in x- and y-direction. The default computational domain is set to 300×150, which is scaled by the induction

length of one-dimensional ZND detonation. The wedge tip is set to $x = 5$ to ease the simulation setting and eliminate the non-physical oscillations near the wedge vertex. A steady ODW is first simulated as the initial flow field, whose transition from an OSW to an ODW may be either abrupt or smooth depending on M_0. Once a steady ODW is established, a sinusoidal density disturbance enters the domain through the left and upper boundaries, which are given as inflow boundary conditions, and the thermodynamic parameters at different instants are set according to the formula $\rho = \rho_0 [1+A \cdot \sin(\omega t)]$. Outflow conditions extrapolated from the interior are implemented on the right boundary. A slip boundary condition is used on the wedge surface starting from $x = 5.0$. The lower boundary before the wedge vertex is set to an outflow condition, which has been verified to be a practical method to deal with the wedge tip flow[3,5,6,8,15,24]. With the inflow density disturbed, the temperature is adjusted accordingly while the velocity and pressure are kept constant. The justification is that the density/temperature disturbance can maintain the same until across the detonation/shock front. If we disturb the inflow pressure, the inflow disturbance parameters could be out of control due to the pressure driven flows, which in turn could pose a great challenge for the analysis of flow features. The inflow velocities, u and v, are calculated and projected according to the steady ODW parameters.

A continuous sinusoidal model is used to mimic the disturbance input. The sinusoidal signal represents the simple but fundamental element for a complex situation. More realistic disturbance can be disassembled into a series of simple sinusoidal signals that are appropriate for the purpose of basic research. Besides, the range of disturbance amplitude/frequency is chosen by reference to the induction length and the oscillating frequency of cellular detonation[30]. In previous studies[26,27], the ratio of induction length to heat release length is a critical parameter controlling the instability of a detonation. By introducing a particular disturbance to the reaction zone, we can examine more

closely the response of detonation dynamic features under periodic inflows.

It is also worth noting that the inviscid assumption may deviate from an intrinsic feature of the realistic flows in one's first impression. The viscous diffusion dominates the flow mechanism due to a small Reynolds number, Re for a low-speed flow. The ODW is attached on a wedge in the open space and the inflow Mach number ranges from 9.0 to 10.0 in this study. According to the previous studies[18,19] , the value of Re is very high in the ODW or other detonation study. The dissipation of the viscosity source almost has no effects on the common features of cellular detonation waves. The main error may be induced by the boundary layer along with the wedge surface, especially for the situation in which there exists an interaction between a shock wave and boundary layer. Nevertheless, for a hypersonic flow, the thickness of the boundary layer on a flat wedge is too thin to affect the ODW fields for most cases. Hence, the inviscid assumption is considered and the slip boundary is applied to mimic the wedge surface. Besides, we are trying to obtain the basic ODW structure and examine the interaction between intrinsic instability and external disturbance under unsteady flow. More quantitative research might include the viscous effects for some realistic situations.

A steady ODW with a certain M_0 and wedge angle $\theta = 30°$ is first simulated as the initial flow field. This study uses the three M_0 values (10.0, 9.5, and 9.0) and the fundamental ODW structures of abrupt and smooth type are shown in Appendix A. Two disturbance parameters, the amplitude A and circular frequency ω, are considered to complete the flow disturbance. The amplitude A varies among 0.2, 0.1, and 0.05. Consistent with the description from the previous study[24], a derived parameter N is interpreted as the number of disturbance cycles in the induction zone. The induction length L_{ini}, along the inflow direction, is defined as the distance between the wedge vertex and the reaction onset on the wedge surface. Hence, the disturbance wavelength can be represented as:

$$\lambda = \frac{L_{ini}}{N} \tag{4}$$

with the disturbance period $T_d = 2\pi/\omega$ and the wavelength $\lambda = U \cdot T_d$, where ω is the disturbance circular frequency and U is the inflow velocity of the steady ODW, which depends on the inflow Mach number and specific heat. Hence, we can obtain the relationship ω and N as follows: $\omega = N \cdot 2\pi U/L_{ini}$. Table 1 lists the values of L_{ini} and ω for three undisturbed ODW structures with their transition types. To improve the readability of this paper, the definitions of some acronyms and a summary list for all test cases are presented in Appendix B.

TABLE 1. Induction length, disturbance circular frequency, and transition type of the steady ODW

M_0	L_{ini}	ω	Type
10.0	23.9	2.88N	smooth
9.5	30.7	2.13N	smooth
9.0	40.9	1.51N	abrupt

3. Results and discussion

3.1 Dependence of dynamic structures on M_0

A total of nine combinations of M_0 and A values were investigated. For each case, there are actually several resulting flow fields depending on N. To facilitate the discussion, the cases are numbered in Table 2, within which the only case addressed[24] previously is case 3 with $M_0 = 10.0$ and $A = 0.2$.

TABLE 2. Case numbers and their M_0 and A values

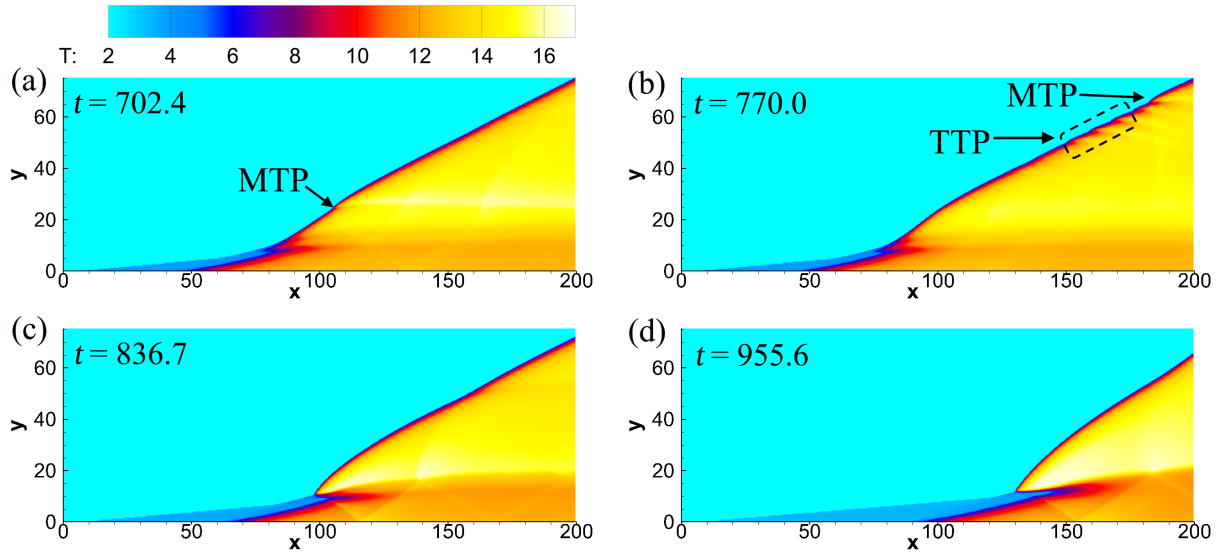| Case No.	$M_0 = 9.0$	$M_0 = 9.5$	$M_0 = 10.0$
$A = 0.2$	case 1	case 2	case 3
$A = 0.1$	case 4	case 5	case 6
$A = 0.05$	case 7	case 8	case 9

FIG. 2. Temperature flow fields of case 1 and $N = 0.01$ at $t =$ (a) 702.4; (b) 770.0; (c) 836.7; (d) 955.6.

A series of ODW simulations with different N were performed for case 1: $M_0 = 9.0$ and $A = 0.2$, and Figs. 2–4 show the typical flow fields with $N = 0.01$, 0.05, and 0.20. Owing to the periodic inflow, the ODW oscillates around the equilibrium position with its structure changing with time. The inflow results in a quasi-steady ODW motion when N is very small, less than 0.01, and the flow fields vary between the static structures. Nevertheless, the unsteady effects become prominent when N increases. With $N = 0.01$, triple points form as shown in Fig. 2 for a disturbance cycle after $t = 700$. In Fig. 2a, the ODW is upstream from its initial equilibrium position, and the abrupt transition changes into the smooth type. One triple point, marked as the MTP (main triple point), remains on the surface. Its formation is due to the surface distortion by unsteady inflow. This MTP is inflow-induced and deterministic, which is different from those generated randomly in the downstream region from the intrinsic instability[12–14]. Subsequently, the MTP and the whole ODW structure move downstream (see Figs. 2b and 2c), with the ODW at an extreme downstream position in Fig. 2d. After the Fig. 2d, the flow structures revert to Fig. 2a and complete a cycle. When the MTP moves downstream in Fig. 2b, however, there is a TTP after the MTP. The TTP is different

from the MTP although both of them result in distorted surfaces. The MTP has only one triple point, which derives from the inflow disturbance. In contrast, the TTP is composed of multi-triple points that arise almost simultaneously and travel together, rather than the isolated triple point in the MTP. This phenomenon has not been observed before to our knowledge and will be analysed in a later section.
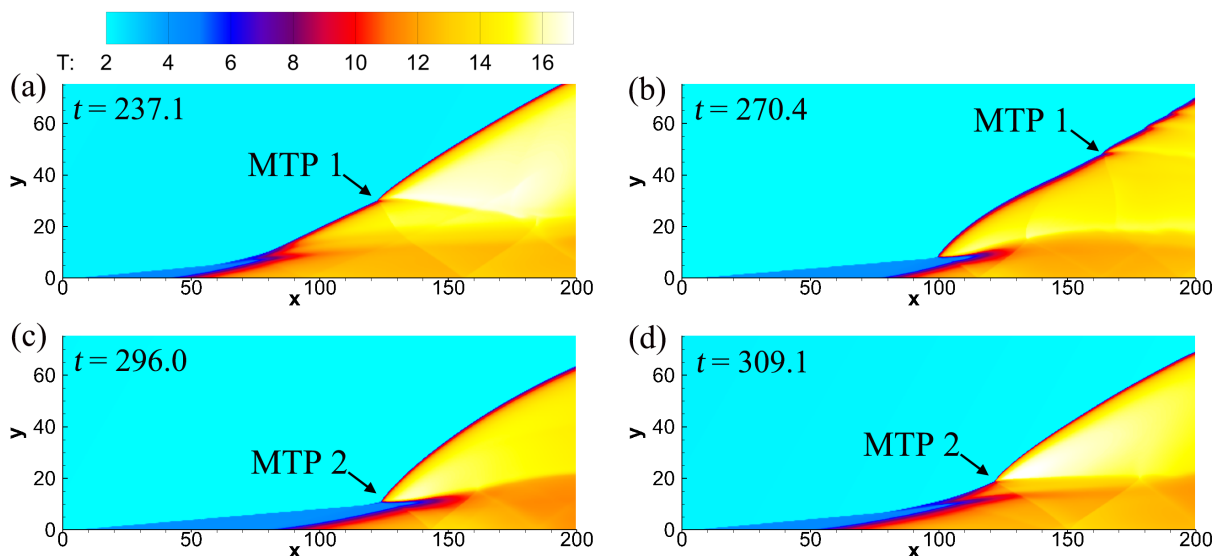

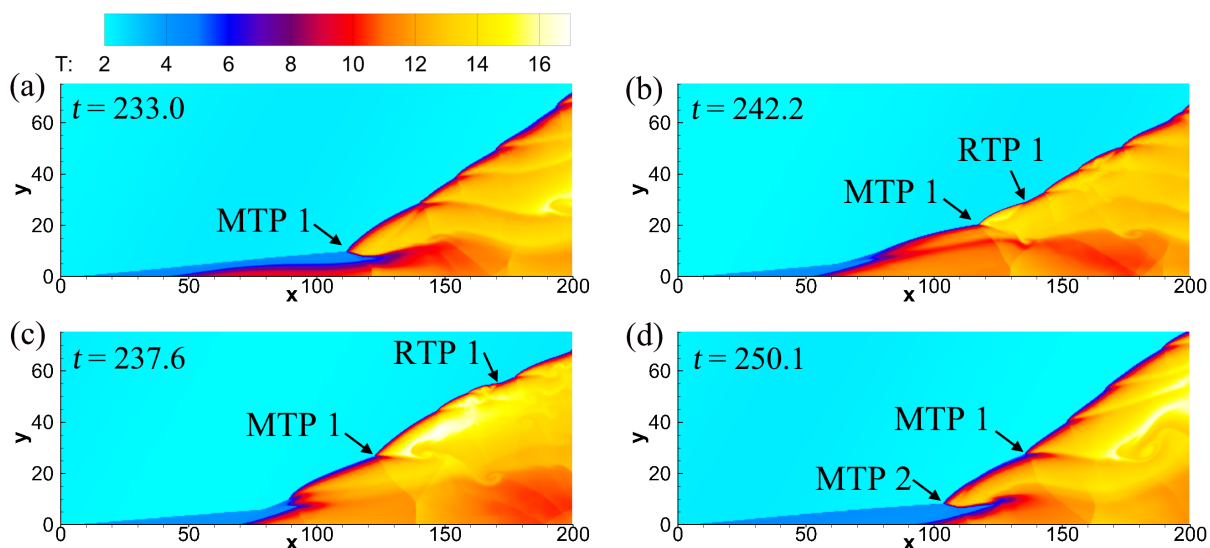FIG. 3. Temperature flow fields of case 1 and $N = 0.05$ at $t =$ (a) 237.1; (b) 270.4; (c) 296.0; (d) 309.1.

FIG. 4. Temperature flow fields of case 1 and $N = 0.20$ at $t =$ (a) 233.0; (b) 242.2; (c) 237.6; (d) 250.1.

Increasing N induces different surface evolution processes. A similar process characterised by MTP formation is observed with $N = 0.05$, as shown in Fig. 3. Two MTPs, MTP1 and MTP2, appear, but the former is generated from the last cycle. Hence, only one triple point (MTP2) forms in the displayed cycle, which is consistent with $N = 0.01$. Nevertheless, the downstream surface near each MTP becomes more unstable with a TTP extending to a subsequent MTP (Fig. 3b). More unstable structures are observed with $N = 0.20$, as shown in Fig. 4. Besides the MTP facing upstream, a reverse triple point (RTP) is also generated with the transverse wave facing downstream. Meanwhile, only one MTP forms in a cycle despite that the surface looks strongly unstable. Triple points formation becomes regular; the flow fields vary with a fixed cycle so that the unsteady ODW is dominated primarily by periodic inflow. Increasing N further in case 1 induces surfaces that are more complicated but qualitatively similar to those of Fig. 4.

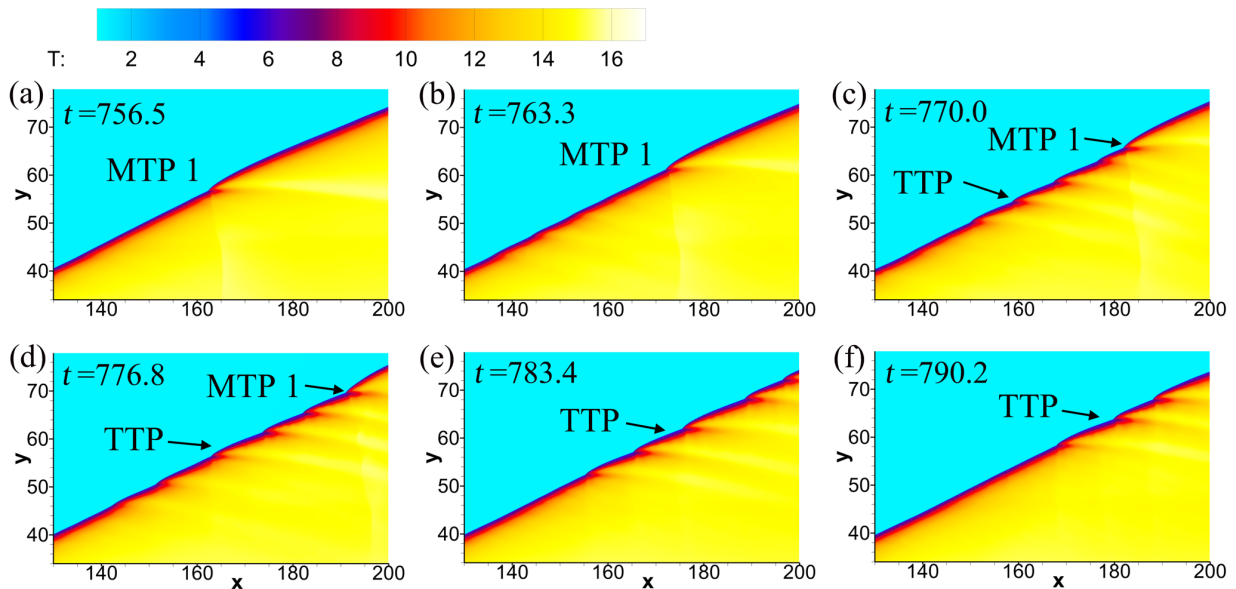## 3.2 Discussion on surface destabilisation

FIG. 5. Evolution of unstable surface with temperature for case 1 with $N = 0.01$: (a) $t = 756.5$; (b) $t = 763.3$; (c) $t = 770.0$; (d) $t = 776.8$; (e) $t = 783.4$; (f) $t = 790.2$.

Triple point formation is critical to describing the ODW in periodic unsteady inflow. The MTP

and RTP observed are similar to those initially with a smooth OSW–ODW transition[24], but the TTPs have not been previously reported. To analyse this feature further, we plot the zoomed-in temperature fields in Fig. 5 with closer time frames for $N = 0.01$. The surfaces before and after the MTP are initially smooth in Fig. 5a. Four triple points then form at almost the same time after the MTP sweeps the smooth surface, as shown in Figs. 5b to 5d. Thereafter, the TTP travels downstream (Figs. 5e and 5f), and the surface returns to being smooth. Considering the TTP appears in each cycle repeatedly, the formation should be closely connected with the disturbance from inflow unsteadiness. However, given a small N, less than 0.01, the disturbed surface swept by the MTP is not significantly destabilised without the grown TTP observed.
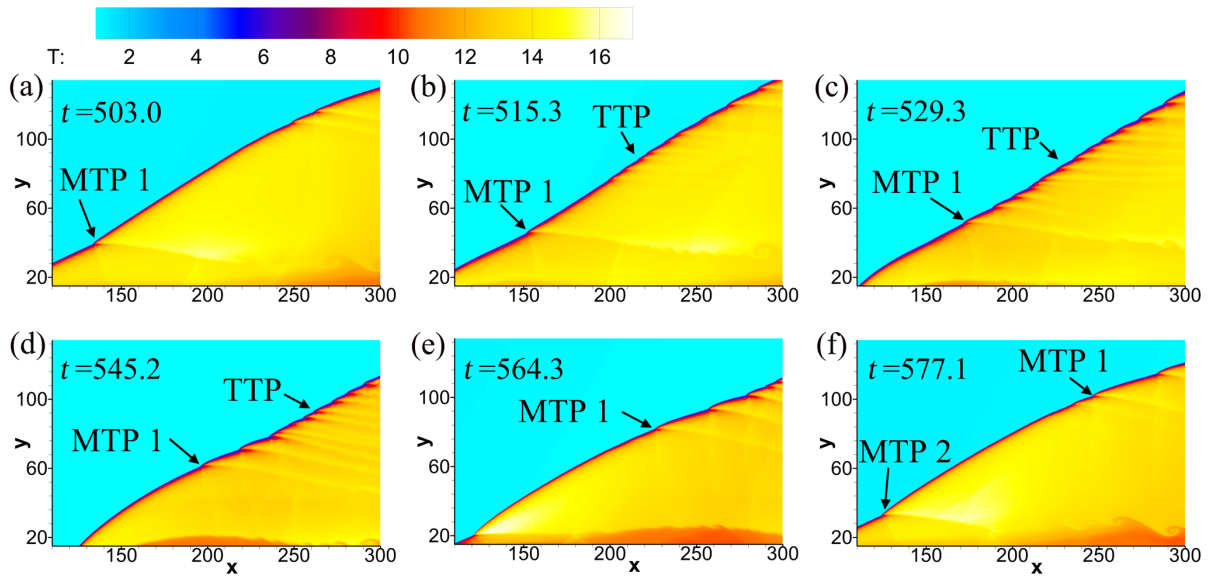

FIG. 6. Evolution of unstable surface with temperature for case 1 with $N = 0.05$: (a) $t = 503.0$; (b) $t = 515.3$; (c) $t = 529.3$; (d) $t = 545.2$; (e) $t = 564.3$; (f) $t = 577.1$.

When N is increased to 0.05 in case 1, the TTP also appears but leads to different wave dynamics. In Fig. 6, a more noticeable bow curve can be seen after the MTP, indicating a strong ODW. The high wave strength initially suppresses the instability. Once this strong ODW relaxes, the surface becomes unstable and a series of triple points appear. Such a TTP extends all the way to the

MTP generated from the next cycle. When the MTP moves downstream and collides with the TTP, the resulting MTP strengthens as indicated by the smooth bow surface after the sweep. Nevertheless, the surface evolution depends on N, resulting in different destabilised processes and TTP positions than those for $N = 0.01$. We also observe that the TTP appears in each cycle repeatedly, suggesting the effects of inflow unsteadiness.
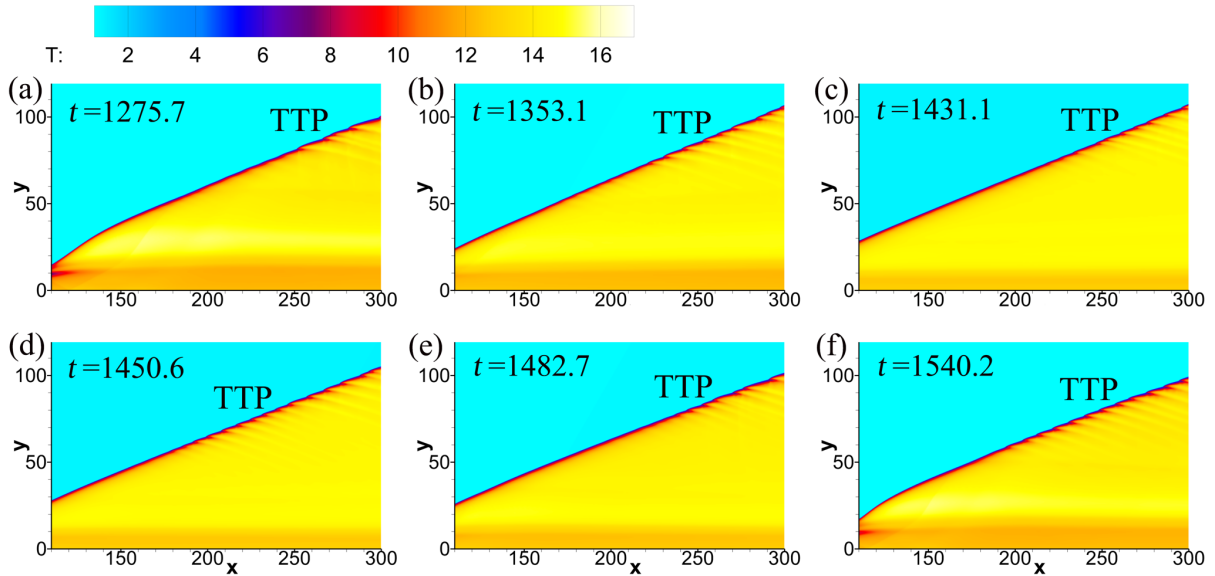

FIG. 7. Evolution of unstable surface with temperature for case 2 with $N = 0.01$: (a) $t = 1275.7$; (b) $t = 1353.1$; (c) $t = 1431.1$; (d) $t = 1450.6$; (e) $t = 1482.7$; (f) $t = 1540.2$.
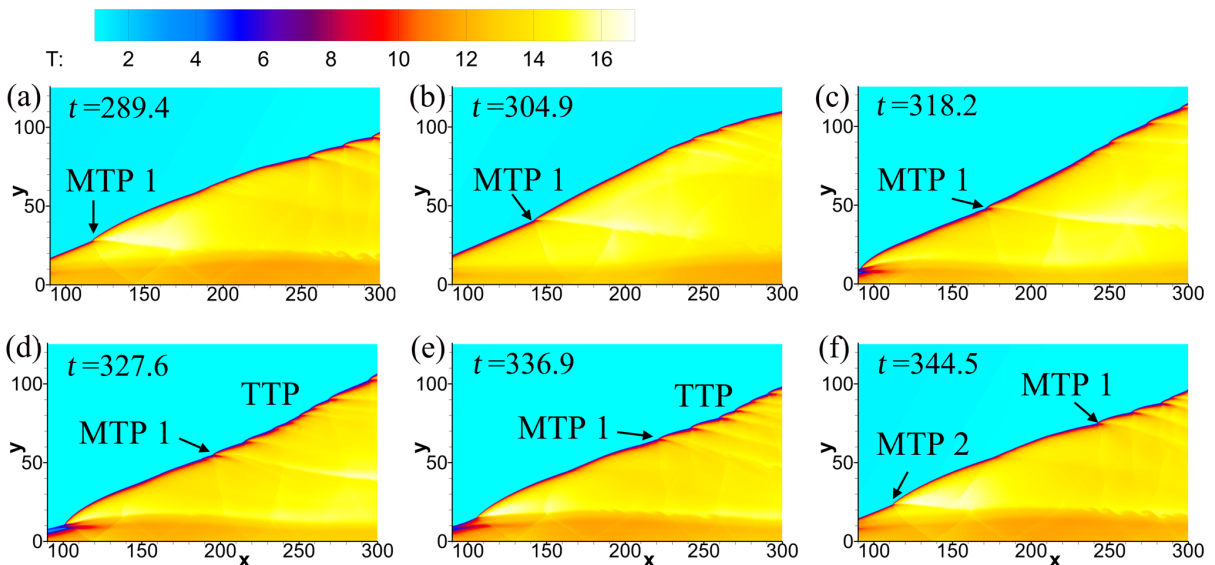

FIG. 8. Evolution of unstable surface with temperature for case 2 with $N = 0.05$: (a) $t = 289.4$; (b) $t =$

304.9; (c) $t = 318.2$; (d) $t = 327.6$; (e) $t = 336.9$; (f) $t = 344.5$.

The ODWs in case 2 by increasing M_0 to 9.5 and keeping A at 0.2 are simulated for different N values. Typical flow fields with $N = 0.01$ and 0.05 are displayed in Figs. 7 and 8. A TTP is observed with $N = 0.01$ in Fig. 7, but there are surprisingly no MTPs. Another difference is that the TTP does not sweep down, but persists on the surface. The TTP in Fig. 7 may travel upstream or downstream depending on the phase of the disturbance. The surface dynamics with $N = 0.05$ in Fig. 8 is close to that in Fig. 6, featuring both the MTP and the TTP. This unsteady ODW and those with higher N, such as 0.20, are all similar to the corresponding ones in case 1, and so are not detailed here.

Further increasing M_0 to 10.0 (keeping A at 0.2) leads to case 3. This case has been studied systematically before, so the flow fields are not displayed here. Generally, case 3 has neither the MTP nor the TTP with $N = 0.01$. Increasing N may induce unstable surfaces with MTPs, but no TTP is observed[24]. Comparing cases 1 to 3, the MTP and TTP determine the main features of the unstable surfaces, thus providing a classification criterion despite the various unstable surfaces resulting from different M_0 and N values. Table 3 indicates whether the MTP or TTP appears in different cases with three typical N values. The MTP forms regardless of N in case 1, but a high N of 0.20 is necessary in case 3. The TTP does not form in case 3 regardless of N, nor does it form with $N = 0.20$ in cases 1 and 2. Two extreme flow fields arise with $N = 0.01$: both the MTP and TTP form in case 1, but neither form in case 3. On the whole, these results demonstrate that the surface is easily destabilised by the MTP at low M_0 and overdrive degree, as discussed elsewhere[13,14]. Meanwhile, the TTP is suppressed by high N, as shown in the last column of Table 3. The obvious differences between MTP and TTP formation can be viewed in Table 3, suggesting the different destabilisation mechanisms of these two structures are related to triple points.

TABLE 3. MTP and TTP appearance in cases 1–3

MTP/TTP	$N = 0.01$	$N = 0.05$	$N = 0.20$
Case 1	YES / YES	YES / YES	YES / NO
Case 2	NO / YES	YES / YES	YES / NO
Case 3	NO / NO	NO / NO	YES / NO

3.3 Effects of inflow disturbance amplitude

Table 2 shows more case simulations with different values for A, the inflow disturbance amplitude. Cases 4 to 6 correspond to $A = 0.1$, and cases 7 to 9 correspond to $A = 0.05$. The cases with $M_0 = 10.0$ are shown in Fig. 9 to illustrate the effects of A. Cases 3, 6, and 9 correspond to $A = 0.2$, 0.1, and 0.05, respectively. The surfaces with $N = 0.10$ in Figs. 9a to 9c demonstrate that decreasing A suppresses MTP formation. There are two MTPs in Fig. 9a but only one in Fig. 9b. Only a weak wrinkled surface is observed when A decreases further to 0.05 in Fig. 9c. With $N = 0.40$ in Figs. 9a to 9c, the surfaces in the same case become significantly unstable, and the effects of A are also clear. There are a few triple points due to high N, and two RTPs form in Fig. 9d. As A decreases in Figs. 9e and 9f, fewer RTPs form and the fine structures become regular. These results demonstrate that for given M_0 and N, the surface is relatively stable for low A and unstable for high A. The other cases, with $M_0 = 9.5$ and 9.0, have similar trends and so are not shown here.
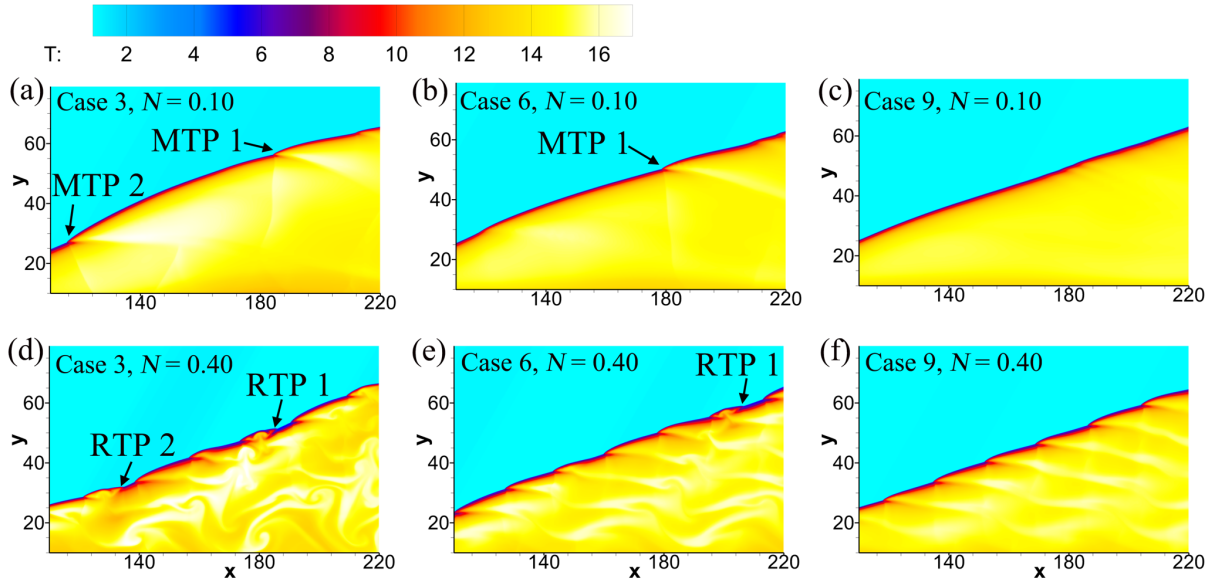
FIG. 9. Temperature flow fields for case 3 (a, d), case 6 (b, e) and case 9 (c, f) with $N = 0.10$ and 0.40

TABLE 4. TTP appearance in cases 1–9 with $N= 0.01$–0.05

TTP	$M_0 = 9.0$	$M_0 = 9.5$	$M_0 = 10.0$
$A = 0.2$	YES	YES	NO
$A = 0.1$	YES	YES	NO
$A = 0.05$	YES	YES	NO

The effects of A on the surface instability above are mainly on MTP formation. The RTP deriving from the MTP is also involved, but TTP formation is not observed in Fig. 9. This is because the corresponding M_0 is high and the wave surface is highly overdriven by the sweeping of the MTP and there is not enough time for the TTP to develop or the overdriven surface to relax[29]. When M_0 decreases to 9.5 or 9.0, the TTP is observed easily. The flow fields of those unstable surfaces are not displayed here owing to their similarity, but Table 4 indicates whether the TTP appears in cases 1–9. It should be noted that high N suppresses TTP formation in all cases, so only the ODWs with $N =$ 0.01–0.05 are considered here. Obviously, a low M_0 is critical to generating the TTP, which

disappears in cases with $M_0 = 10$ in the last column. Surprisingly, the amplitude A does not influence

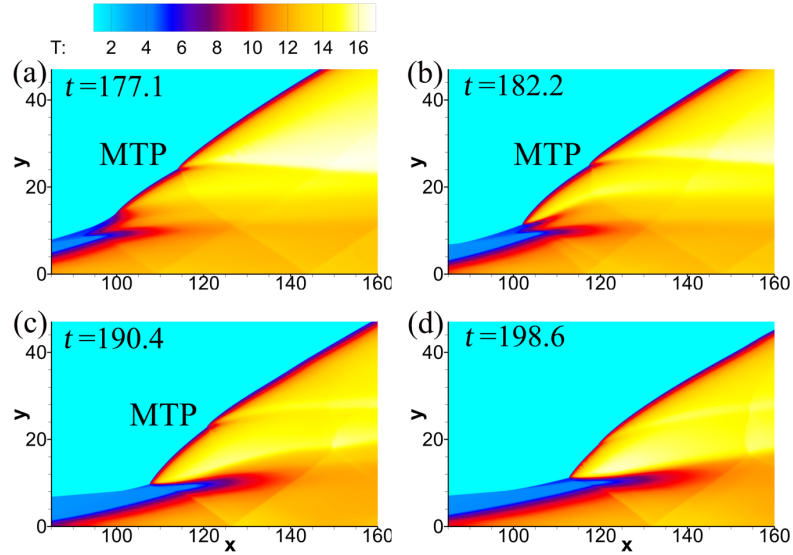the TTP, which suggests essential differences from MTP formation.

FIG. 10. Evolution of unstable surface with temperature for case 4 with $N = 0.10$: (a) $t = 177.1$; (b) $t = 182.2$; (c) $t = 190.4$; (d) $t = 198.6$.
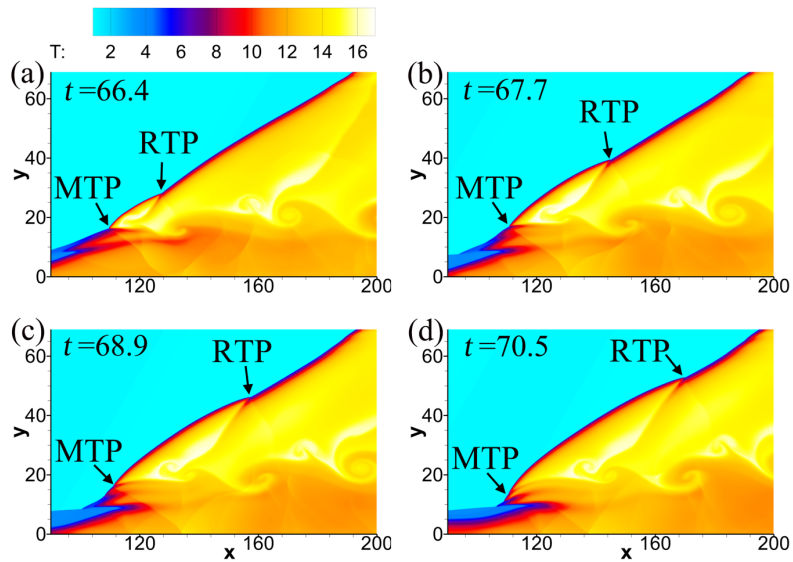

FIG. 11. Evolution of unstable surface with temperature for case 4 with $N = 0.40$: (a) $t = 66.4$; (b) $t = 67.7$; (c) $t = 68.9$; (d) $t = 70.5$.

Besides the MTP and TTP formation discussed above, meaningful wave dynamics are observed in case 4, $M_0 = 9.0$ and $A = 0.1$. As shown in Fig. 10, MTP formation is observed initially with $N = 0.10$, but the MTP evolves differently from before and does not sweep downstream or travel downstream. Nevertheless, the persisting MTP cannot last for over one cycle, but subsequently degenerates and becomes wrinkle-like on the surface, as shown in Fig. 10. This process happens with a wide N range, as low as 0.02, and further decreasing N to 0.01 leads to a surface without an MTP. Meanwhile, increasing N to 0.20 results in a similar degeneration. A slightly different process happens with $N = 0.40$ in case 4, as shown in Fig 11. Both the MTP and RTP appear on the surface, owing to the high N. The MTP still appears and degenerates similarly, while the RTP sweeps the surface downstream.

The MTP degeneration illustrates a novel, unsteady wave dynamics not observed before, though there is a process that may be related to it in the previous study[24]. In the case $M_0 = 10.0$, $A = 0.2$, and $N = 0.05$, the surface of the unsteady ODW stays smooth, while the MTP arises given a single-pulse disturbance. This suggests a proper disturbance may weaken triple point formation in the next cycle. This could explain why the degeneration happens, so it is necessary to clarify the conditions under which the degeneration does. Undoubtedly, the degeneration requires a proper MTP persisting near the initiation region, so such dynamics is absent in cases with high M_0. However, A is also critical to get a proper MTP: in case 1, A is too large, so the MTP is strong and travels downstream soon; in case 7, A is too small, so the MTP does not appear. This preliminary analysis indicates that MTP degeneration requires several strict conditions that are rarely observed.

3.4 Analysis of unsteadiness features

The resulting unsteady ODWs above are complicated owing to the effects of periodic inflow,

leading to different structures and dynamics from those in steady inflow. The periodic inflow is critical to the surface instability, whose effects have been investigated using the bifurcation parameters M_0, A, and N. This study extends the previous work with fixed M_0 and A [24], leading to a complete understanding of surface instability. It was previously demonstrated that MTP formation could be achieved easily with high N. The present study not only verifies it but also indicates that the MTP is easily triggered with high A and low M_0. The effects of the amplitude A are intuitive physically, while the effects of M_0 are due to the change of surface overdrive degree. Moreover, the MTP degeneration in the unsteady ODW is observed when there is a proper disturbance with modest A and low M_0. However, the newly observed TTP formation exhibits special features and deserves more attention. Tables 3 and 4 show that TTP formation is sensitive to M_0 and N but not to A. However, it neither appears for $M_0 = 10$ nor for high N. The TTP and MTP formations depend on the same series of parameters, i.e., M_0, N, and A, but with obviously different dependences.

We analyse the frequency features of the surface oscillation to clarify the TTP formation mechanism. The oscillations of reactive front positions were first recorded as functions of time for several cycles, generating a time series. Then, the power spectral density (PSD) was computed via an FFT (Fast Fourier Transformation) of the autocorrelation sequence of the time series, which can be considered the power distribution over frequencies. Figures 12 and 13 show the results for case 1 with $N = 0.20$ and case 2 with $N = 0.01$, respectively. The flow fields for these two cases are illustrated in Figs. 4 and 7. These cases are chosen because the former has only the MTP on the surface, while the latter has only the TTP on the surface. In Figs. 12 and 13, the inset with a grey background is the magnified region near the x-axis to display the difference there clearly.
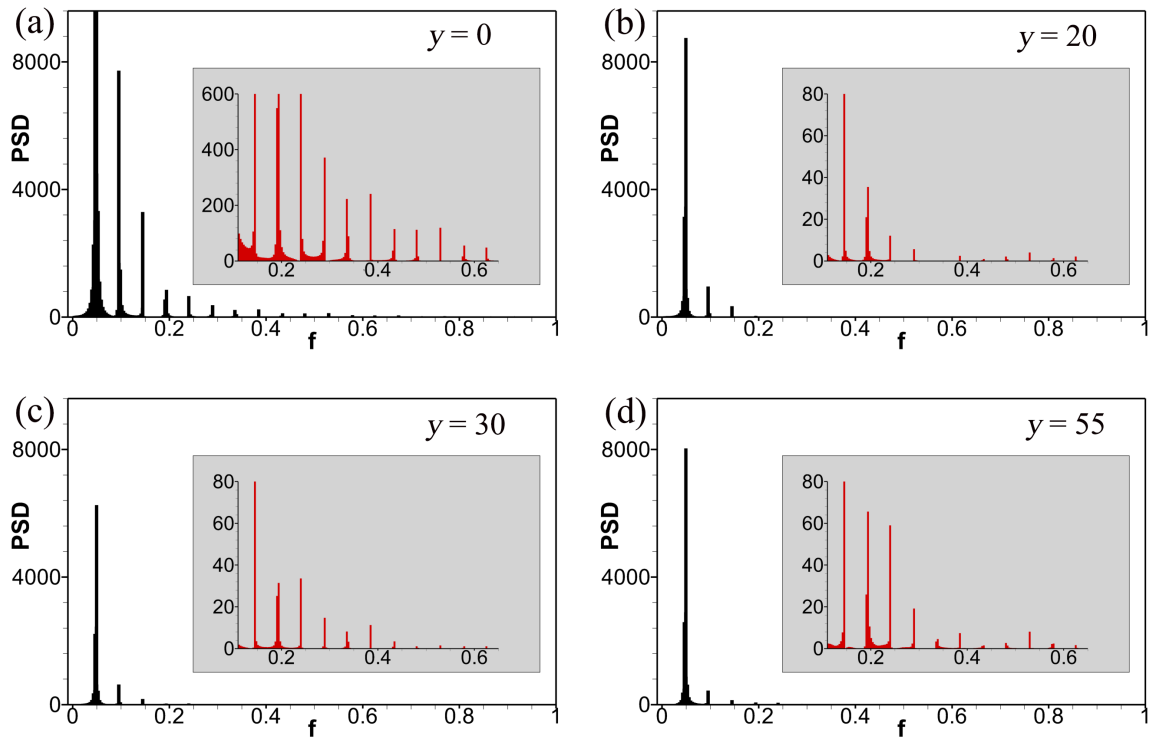
FIG. 12. PSDs of reactive front oscillations along different lines parallel to the x-axis in case 1 with

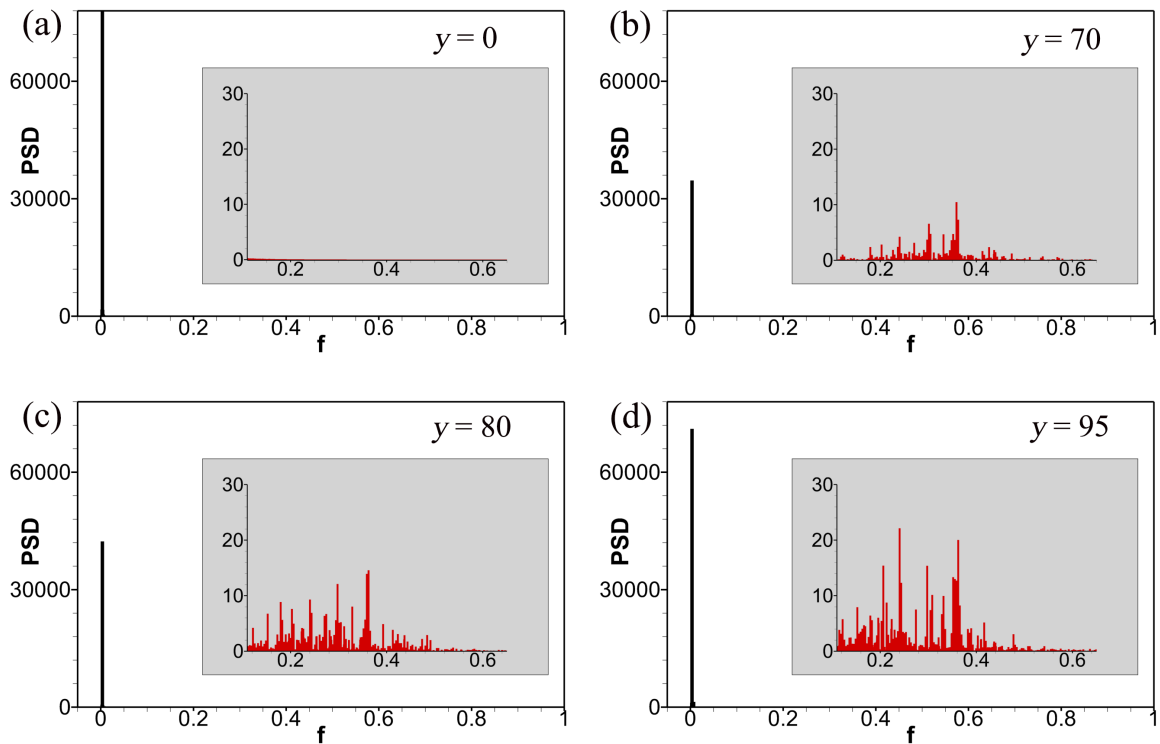$N = 0.20$: (a) $y = 0$; (b) $y = 20$; (c) $y = 30$; (d) $y = 55$.

FIG. 13. PSDs of reactive front oscillations along different lines parallel to the x-axis in case 2 with

$N = 0.01$: (a) $y = 0$; (b) $y = 70$; (c) $y = 80$; (d) $y = 95$.

For case 1 with $N = 0.20$, Fig. 12 shows a dominant frequency determined by N. The dominant

frequency corresponds to the highest PSD in all the frames, staying the same along different lines.

There are several other harmonic peaks in each frame whose frequency corresponds to certain times

of the dominant one. The dominant frequency and its harmonics are due to the post-shock

disturbance in the initiation region and so arises in Fig. 12a. When the monitored surface location

moves downstream, the PSDs of every frequency decrease from Figs. 12a to 12c and increase again

in Fig. 12d, illustrating different oscillation strengths. Nevertheless, both the dominant frequency and

its harmonics stay the same, and no new frequencies are observed. This demonstrates that the MTP is

powered by the upstream inflow as a forced destabilisation. Furthermore, the resulting ODW

evolution shows that the MTP is mainly originated from the initiation zone near the detonation front.

Under the period flow, the OSW gets bent, but keeps the surface smooth; no triple point forms on the

wave front. However, the heat release reaction along the wedge surface is sensitive to inflow

temperature disturbance. The oscillatory reactive front interacts with the detonation front, which

results in the formation of MTP. Then, the MTP sweeps through the surface or degenerates near the

initiation region.

An essentially different frequency behaviour is observed for case 2 with $N = 0.01$, as shown in

Fig. 13. First, there is also one dominant frequency in each frame. This frequency is very close to 0

because of a smaller N, and its harmonics are absent, generating an isolated dominant frequency in

Fig. 13a. Nevertheless, a frequency spectrum arises gradually from Figs. 13b to 13d, exhibiting a

different oscillation behaviour as compared to the last case. This frequency spectrum only appears in

the cases of TTP formation, reflecting the TTP effects on the surface oscillation. The previous study[30]

also demonstrated that a frequency spectrum without obvious dominant frequencies is induced by the

random formation of triple points on the unstable surface, whose destabilisation derives from the intrinsic instability. Thus, this frequency spectrum suggests that the intrinsic instability plays an important role in surface evolution, which is different from the MTP formation induced by forced destabilisation. In this dynamics situation, the surface with $M_0 = 9.0$ is actually unstable, but the destabilisation manifests slowly until it accelerates with the help of the inflow disturbance. Therefore, the TTP formation is the combined effect of ODW surface instability and inflow disturbance.

The surface oscillation reflects another unsteady feature of these ODWs in periodic inflows. To quantify the oscillations, we calculate the surface movement amplitude A' along lines parallel to the x-axis according to their extreme positions. Figure 14 shows typical results corresponding to cases 1 ($M_0 = 9$, $A = 0.2$) and 7 ($M_0 = 9$, $A = 0.05$). There are two main features common to both cases. One is that the curve of A' for each N reaches its maximum around the initiation region, so the curve increases first and then decreases. In case 1 with high N, such as 0.20 or 0.40, the maximum A' moves to $y = 0$ owing to the complicated dynamics in the initiation region. The other common feature is that the downstream A', such as that along $y = 60$, increases first and then decreases when N changes, demonstrating the most intense oscillation occurs with a modest N. These phenomena are similar to those observed before[24], indicating that these are the common features of unsteady ODWs.
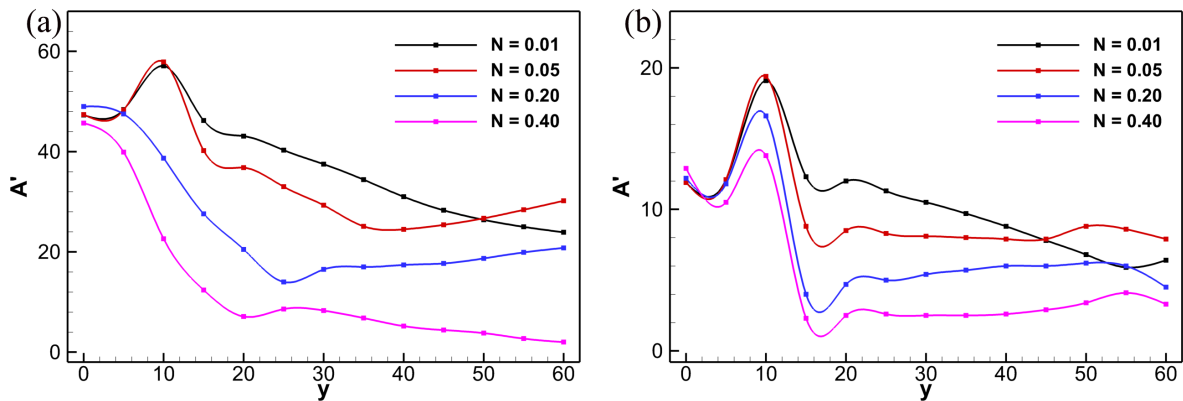

FIG. 14. Oscillation amplitudes depending on y in cases 1 (a) and 7 (b).

The effects of varying A and M_0 are also investigated comprehensively. Comparing two frames of Fig. 14 shows that high A (case 1) leads to a strong oscillation with a large A'. The only exception arises with $N = 0.40$ because the corresponding flow fields of case 1 are very disordered and full of fine wavelets, suppressing the downstream oscillation. The effects of M_0 on the oscillation amplitude A' are complicated because A' depends on its location on the surface, as shown in Fig. 14. Hence, surface locations are chosen to be comparable, i.e., $y = 60$, 45, and 35 for $M_0 = 9.0$, 9.5, and 10.0, respectively. These heights correspond to the comparable downstream surfaces, whose distances to the initiation point are about 5 times the initiation height. The oscillation amplitudes along $y = 0$ are compared with the downstream A', as shown in Fig. 15. It is obvious that for all the 9 cases, A' along $y = 0$ depends on M_0 and A but is not sensitive to N. Meanwhile, the downstream A' always increases and reaches a peak around $N = 0.1$. More importantly, M_0 clearly influences the relation between the two curves in Fig. 15. With $M_0 = 9$, the downstream A' stays lower than the A' along with $y = 0$, as shown in the first column. When M_0 increases to 9.5 in the second column, the peak of the downstream A' increases over the corresponding A' along with $y = 0$. In the third column, there is a wide range in which the downstream A' is larger than the A' along $y = 0$.
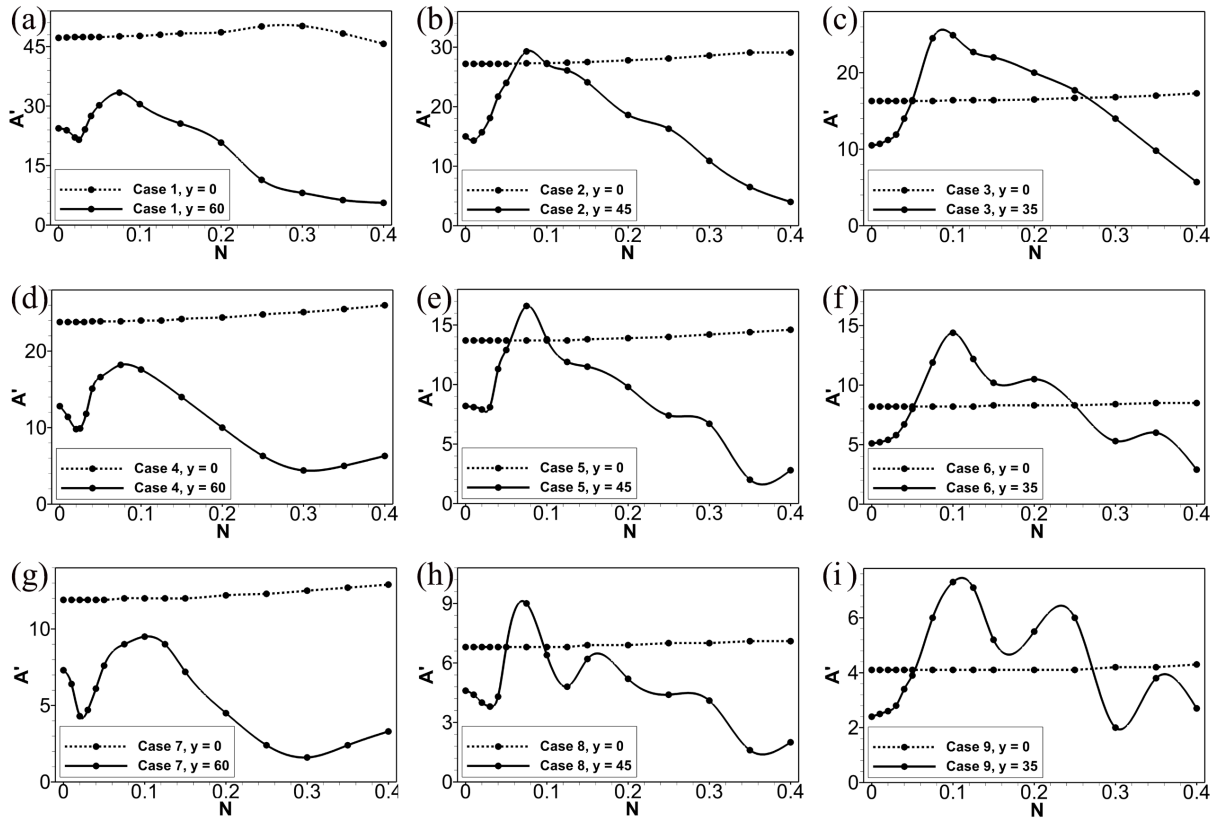
FIG. 15. Oscillation amplitudes as functions of N along two lines parallel to the y-axis. Frames (a)–(i) correspond to cases 1–9.

The two-curve relation in Fig. 15 shows the effects of M_0, or transition type, on the surface oscillation. The A' along $y = 0$ represents the oscillation of the shock-induced ignition. The streamline along $y = 0$ is achieved by a self-ignition in the shocked gas, which is influenced only by the inflow unsteadiness. Meanwhile, the downstream A' in Fig. 15 represents the oscillation of ODW surfaces, an effect not only of its pre-shock unsteady inflow but also the disturbance from the upstream surfaces. Then, we could conclude from these results that the oscillation of the ODW surface has been weakened from upstream to downstream when $M_0 = 9$ and strengthened when $M_0 = 10$. These variations along the surface only occur with a modest N, and high N leads to weakening regardless of M_0. In general, the difference should be attributed to the transition structure determined by M_0. An abrupt transition appears when $M_0 = 9$, while a smooth transition arises when $M_0 = 10$. The

abrupt transition involves a multi-shock wave system that dampens the downstream oscillation, while the smooth transition does not dampen. This also explains why high N always leads to weakening, since the complicated shock systems form in the initiation region. The weak oscillation downstream is favourable for ODE application and is easily controlled and regulated. This suggests the abrupt transition is a good choice from the viewpoint of flow stability, although other aspects such as the total pressure loss should be considered collectively.

4. Conclusions

This study introduced continuous disturbance to model unsteady inflows and analyse the resulting ODW dynamics. The results demonstrate TTP formation and MTP degeneration on ODW surfaces for the first time. More importantly, an underlying understanding of surface instability has been developed from the viewpoint of MTP and TTP formation. Parametric study and frequency analysis have revealed that the MTP derives from the forced destabilisation, while the TTP derives from the combined effects of surface instability and inflow disturbance. The oscillation amplitudes of unsteady ODWs were analysed with respect to M_0 and inflow disturbance, demonstrating the effects of transition type on the downstream oscillation amplitude. These findings complete the preliminary work [24], which was based on fixed values of M_0 and A. The unstable ODW structures bring new challenges to the operation of ODEs. From the viewpoint of practical applications, a stationary ODW is required to achieve steady combustion, but many recent studies[9,12,14,30] have shown that the surface of ODW is unsteady due to the presence of triple points. The thermodynamic parameters across the cellular detonation front change sharply, which could play a critical role in the performance of detonation-based propulsion systems. The findings in the present study have confirmed that the unsteady flow could affect significantly the features of an unstable oblique detonation wave front.

Nevertheless, it shows that under the influence of unsteady inflow modeled in this work the detonative combustion process can still operate via quasi-steady wave systems, which could have practical implications.

Finally, a limitation of this study is that only the gas-dynamic parameters are taken into account systematically and the detonation of the chosen reactive mixture parameters is further stabilized due to the overdrive. A more unstable mixture with higher activation energy is needed to fully understand the intrinsic feature of unsteady flow dynamics, especially in some more extreme cases that could cause the failure of a detonation. Furthermore, realistic unsteady inflow models should be implemented in future work. The non-harmonic inflow disturbance may induce more complicated phenomena, yielding fruitful progress in both fundamental research and ODE application.

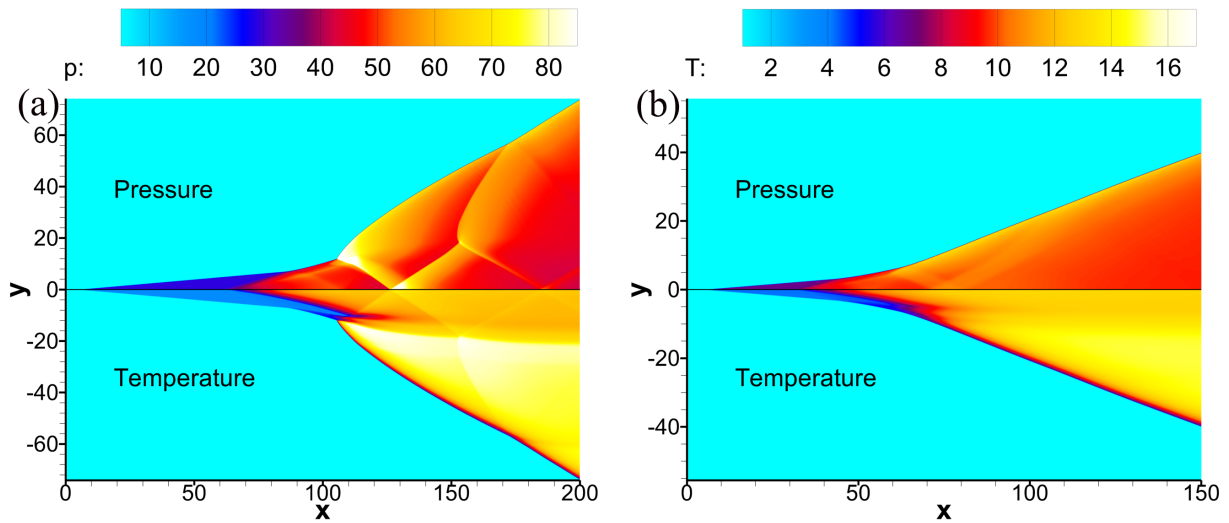## Appendix A: Steady structures and resolution study

FIG. 16. ODW pressure and temperature with $M_0 =$ (a) 9.0 and (b) 10.0.

Two steady cases were simulated to illustrate the fundamental ODW structures. Figure 16 shows the pressure and temperature fields with $M_0 = 9.0$ and 10.0. An abrupt ODW transition arises in Fig. 16a, while a smooth ODW transition arises in Fig. 16b. The former structure is much more complicated than the latter, and complicated multi-wave structures are observed in both the transition regions and the post-surface product. The latter was used as the only fundamental structure in previous study[19] , while both of them and an intermediate one with $M_0 = 9.5$ not shown here have been used in this study.
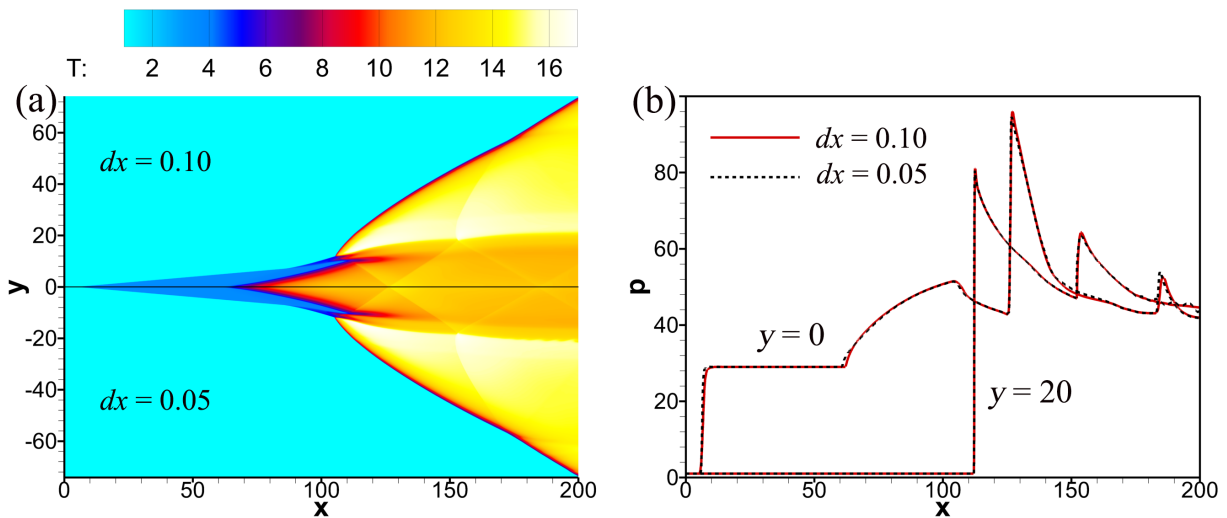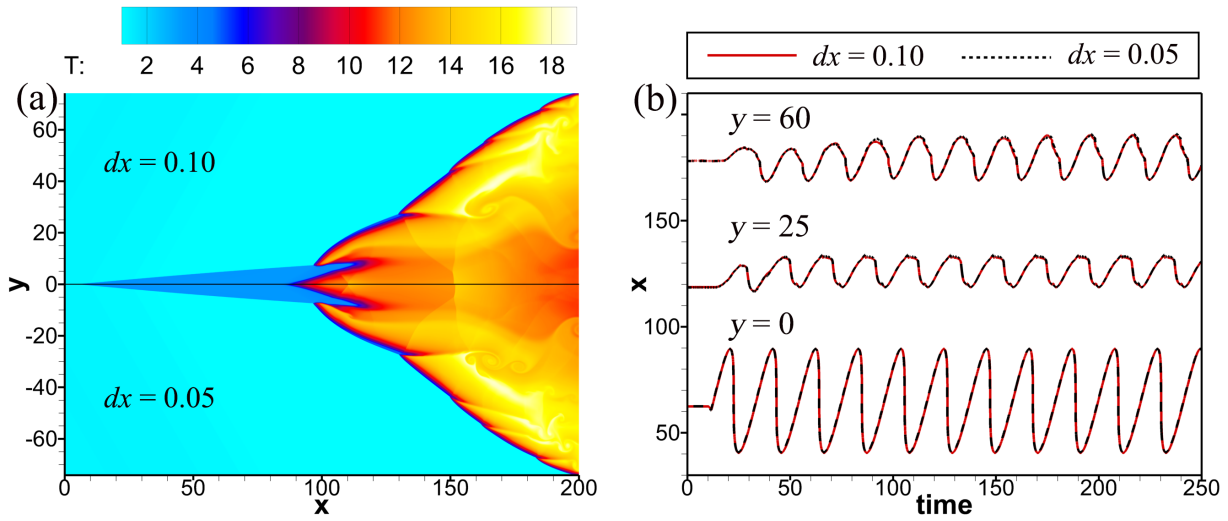
FIG. 18. Temperature contours (a) and reactive front positions (b) for the unsteady ODW of case 1

with $N = 0.20$

To verify the numerical resolution effect, the steady ODW with $M_0 = 9$ was first simulated with

two grid sizes. The flow fields in Fig. 17 are almost the same and the differences are difficult to

distinguish. A quantitative comparison was conducted by plotting the pressure profiles along with the

lines $y = 0$ and 20, as shown in Fig. 17b. Clearly, the curves are overlapped together so the effects of

different grids are found to be negligible. Moreover, the unsteady ODW in case 1 with $N = 0.20$ was

also simulated. Figure 18 shows that the instantaneous ODW keeps essentially the same structure for

the coarse grid, 0.10×0.10, or fine grid, 0.05×0.05. Figure 18b shows the oscillating reactive front

position at different y positions. The reactive front location is defined by the end of the induction

reaction where heat release begins, i.e., $\xi = 0$ and $\eta = 0$. The overlapped curves also show that the

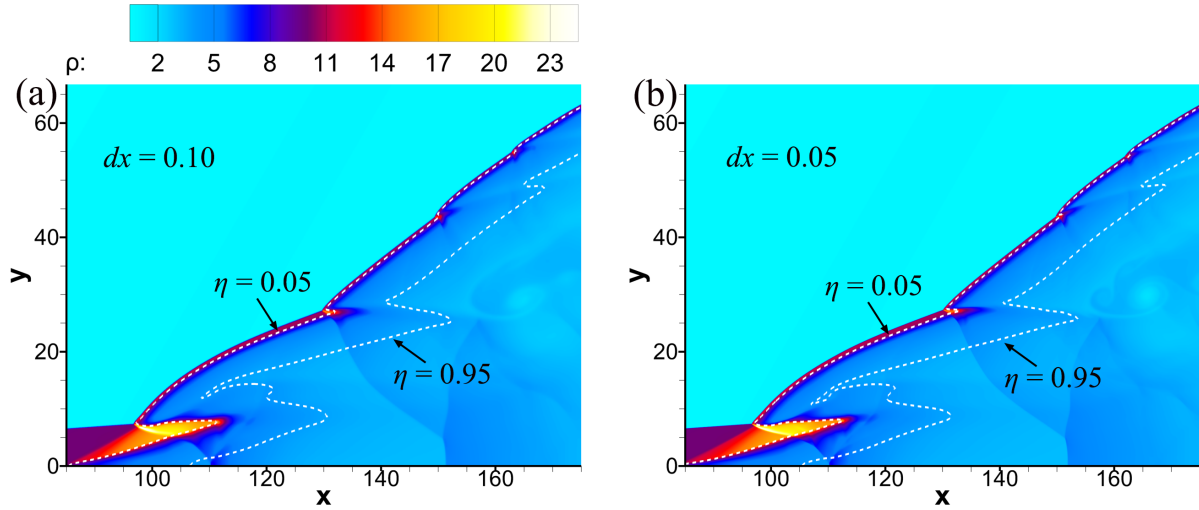periodicity is almost independent of grid size.

FIG. 19 Zoom-in density contours for the unsteady ODW of case 1 with $N = 0.20$, and the white lines denote the progress variables η of the heat release reaction : (a) $dx = 0.10$ and (b) $dx = 0.05$.

Besides, the zoom-in density flow fields near the triple points are represented in Fig. 19. The reaction variable contours are also plotted to identify the main heat release zone. It can be seen from Fig. 19a, that the triple point positions and the shape of wave/reaction front are almost the same as the finer grid of Fig. 19b, expect the fine vortex structures in the detonation product. Overall, the 0.10×0.10 grid was thus deemed enough to capture the detonation surface oscillation and used as the default resolution in this study.

Appendix B: The definition of some acronyms and the summary table for all test cases

In this section, the definitions of some acronyms are shown in Table B1 to enhance readability. The test cases in this study, along with the corresponding figure number are presented in Table B2.

TABLE B1 Table of acronyms

Acronyms	Definition
ODW	Oblique detonation wave

OSW		Oblique shock wave	
MTP		Main triple point	
TTP		Train of triple points	
RTP		Reverse triple point	
PSD		Power spectral density	
FFT		Fast Fourier Transformation	

TABLE B2 The test cases in the present study

Case No.	A	M_0	Figure No.
Case 1	0.2	9.0	Figs. 2–6, Fig. 12, Fig. 15
Case 2	0.2	9.5	Fig. 7, Fig. 8, Fig. 13, Fig. 15
Case 3	0.2	10.0	Fig. 9 Fig. 15
Case 4	0.1	9.0	Fig. 10, Fig. 11, Fig. 15
Case 5	0.1	9.5	Fig. 15
Case 6	0.1	10.0	Fig. 9, Fig. 15
Case 7	0.05	9.0	Fig. 15
Case 8	0.05	9.5	Fig. 15
Case 9	0.05	10.0	Fig. 9, Fig. 15

Data availability

The data that support the findings of this study are available from the corresponding author upon reasonable request.

References

[1] P. Wolański, "Detonative propulsion," Proc. Combust. Inst. **34**, 125–158 (2013).

[2] J. M. Powers, "Oblique detonations: Theory and propulsion applications," in *Combustion in High-Speed Flows* (Springer, 1994), pp. 345–371.

[3] C. Li, K. Kailasanath, and E. S. Oran, "Detonation structures behind oblique shocks," Phys. Fluids **6**, 1600–1611 (1994).

[4] C. Viguier, L. F. Figueira da Silva, D. Desbordes, and B. Deshaies, "Onset of oblique detonation waves: Comparison between experimental and numerical results for hydrogen-air mixtures," Proc. Combust. Inst. **26**, 3023–3031 (1996).

[5] H. H. Teng and Z. L. Jiang, "On the transition pattern of the oblique detonation structure," J. Fluid Mech. **713**, 659–669 (2012).

[6] Y. Liu, Y. S. Liu, D. Wu, and J. P. Wang, "Structure of an oblique detonation wave induced by a wedge," Shock Waves **26**, 161–168 (2016).

[7] Y. Fang, Y. Zhang, X. Deng, H. Teng, "Structure of wedge-induced oblique detonation in acetylene-oxygen-argon mixtures," Phys. Fluids **31**, 026108 (2019).

[8] P. Yang, H. Teng, Z. L. Jiang, and H. D. Ng, "Effects of inflow Mach number on oblique detonation initiation with a two-step induction-reaction kinetic model," Combust. Flame **193**, 246–256 (2018).

[9] W. Han, C. Wang, and C. K. Law, "Three-dimensional simulation of oblique detonation waves attached to cone," Phys. Rev. Fluids **4**, 053201 (2019).

[10] C. Viguier, A. Gourara, and D. Desbordes, "Three-dimensional structure of stabilization of oblique detonation wave in hypersonic flow," Proc. Combust. Inst. **27**, 2207–2214 (1998).

[11] M.V. Papalexandris, "A numerical study of wedge-induced detonations," Combust. Flame **120**, 526–538 (2000).

[12] J. Y. Choi, D. W. Kim, I. S. Jeung, F. Ma, and V. Yang, "Cell-like structure of unstable oblique detonation wave from high-resolution numerical simulation," Proc. Combust. Inst. **31**, 2473–2480 (2007).

[13] J. Verreault, A. J. Higgins, R. A. Stowe, "Formation of transverse waves in oblique detonations," Proc. Combust. Inst. **34**, 1913–1920 (2013).

[14] H. Teng, H. D. Ng, K. Li, C. Luo, and Z. Jiang, "Evolution of cellular structures on oblique detonation surfaces," Combust. Flame **162**, 470–477 (2015).

[15] Z. Ren, B. Wang, G. Xiang, and L. Zheng, "Effect of the multiphase composition in a premixed fuel-air stream on wedge-induced oblique detonation stabilization," J. Fluid Mech. **846**, 411–427 (2018).

[16] J. -Y. Choi, E. J.-R. Shin and I.-S. Jeung, "Unstable combustion induced by oblique shock waves at the non-attaching condition of the oblique detonation wave," Proc. Combust. Inst. **32**, 2387–2396 (2009).

[17] G. X. Xiang, X. Gao, W. J. Tang, X. Z. Jie and X. Huang, "Numerical study on transition structures of oblique detonations with expansion wave from finite-length cowl," Phys. Fluids **32**, 056108 (2020).

[18] K. Wang, Z. Zhang, P. Yang and H. Teng, "Numerical study on reflection of an oblique detonation wave on an outward turning wall," Phys. Fluids **32**, 046101 (2020).

[19] K. Wang, H. Teng, P. Yang and H. D. Ng, "Numerical investigation of flow structures resulting from the interaction between an oblique detonation wave and an upper expansion corner," J. Fluid Mech. **903**, A28 (2020).

[20] K. Iwata, S. Nakaya, and M. Tsue, "Wedge-stabilized oblique detonation in an inhomogeneous hydrogen–air mixture," Proc. Combust. Inst. **36**, 2761–2769 (2017).

[21] Y. Fang, Z. Hu, H. Teng, Z. Jiang, and H. D. Ng, "Numerical study of inflow equivalence ratio inhomogeneity on oblique detonation formation in hydrogen-air mixtures," Aerosp. Sci. Technol. **71** 256–263 (2017).

[22] Y. Liu, L. Wang, B. Xiao, Z. Yan, and C. Wang, "Hysteresis phenomenon of the oblique detonation wave," Combust. Flame **192**, 170–179 (2018).

[23] Y. Zhang, P. Yang, H. Teng, H. D. Ng, and C. Wen, "Transition between different initiation

structures of wedge-induced oblique detonations," AIAA J. **56**, 4016–4023 (2018).

[24] P. Yang, H. D. Ng, and H. Teng, "Numerical study of wedge-induced oblique detonations in unsteady flow," J. Fluid Mech. **876**, 264–287 (2019).

[25] M. Y. Gui, B. C. Fan, G. Dong, "Periodic oscillation and fine structure of wedge-induced oblique detonation waves," Acta Mech. Sin. **27**, 922–928 (2011).

[26] M. Short and G. J. Sharpe, "Pulsating instability of detonations with a two-step chain-branching reaction model: theory and numerics," Combust. Theory Model **7,** 401–416 (2003).

[27] H. D. Ng, M. I. Radulescu, A. J. Higgins, N. Nikiforakis, and J. H. S. Lee, "Numerical investigation of the instability for one-dimensional Chapman–Jouguet detonations with chain-branching kinetics," Combust. Theory Model. **9**, 385–401 (2005).

[28] Z. L. Jiang, "Dispersion-controlled principles for non-oscillatory shock-capturing schemes," Acta Mech. Sin. **20**, 1–15 (2004).

[29] H. H Teng, Z. L. Jiang, and H. D. Ng, "Numerical study on unstable surfaces of oblique detonations," J. Fluid Mech. **744**, 111–128 (2014).

[30] P. Yang, H. Teng, H. D. Ng, and Z. Jiang, "A numerical study on the instability of oblique detonation waves with a two-step induction–reaction kinetic model," Proc. Combust. Inst. **37**, 3537–3544 (2019).